Thermoelectric response of a periodic composite medium in the presence of a magnetic field: Angular anisotropy

Yakov M. Strelniker[1,*] and David J. Bergman[2,†]

[1]*Department of Physics, Bar-Ilan University, IL-52900 Ramat-Gan, Israel*

[2]*Raymond and Beverly Sackler School of Physics and Astronomy, Faculty of Exact Sciences, Tel Aviv University, IL-69978 Tel Aviv, Israel*

(Received 25 September 2017; published 22 December 2017)

A calculational method based on Fourier expansion is developed and applied to the study of the strong-field galvanomagnetic thermoelectric properties of a free-electron metal, inside of which is embedded a simple cubic array of identical spheres or cylinders, which have different thermoelectric and conductivity tensors. When the magnetic field is strong enough, the effective galvanomagnetic thermoelectric properties of such composites exhibit very strong variations with the direction of the applied magnetic field with respect to the symmetry axes of the composite microstructure. This is qualitatively similar to the predicted magnetoinduced angular magnetoresistance anisotropy [D. J. Bergman and Y. M. Strelniker, Phys. Rev. B **49**, 16256 (1994)] which was verified experimentally [M. Tornow *et al.*, Phys. Rev. Lett. **77**, 147 (1996)]. This is a purely classical effect, even though it is qualitatively similar to what is observed in some metallic crystals which have a noncompact Fermi surface. The current results can be useful for studying the possibility of increasing the thermoelectric figure of merit in periodic composites by application of a strong magnetic field. As follows from our very preliminary results, the figure of merit can be increased by application of a strong magnetic field to the composite.

DOI: 10.1103/PhysRevB.96.235308

I. INTRODUCTION

The effects of an externally applied magnetic field **B** on the thermoelectric response of a uniform electronic conductor were first studied in Ref. [1]. Later studies, starting in 1955, were mostly aimed at gaining a better understanding of the microscopic transport processes in metals and semiconductors [2–6]. It was also found that in single crystals of bismuth the Nernst-Ettingshausen magnetothermoelectric effect exhibits a strong dependence on the direction of **B** with respect to the crystal axes [2,7]. An important driving factor in many subsequent studies was the quest for ways to enhance the so-called thermoelectric quality factor or thermoelectric figure of merit [8–10] ZT, which is a dimensionless quantity [11–13]:

$$ZT \equiv \frac{\sigma S^2 T}{\kappa} = \frac{\Delta}{1-\Delta}, \quad \Delta \equiv \frac{T\chi^2}{\sigma\lambda_E}. \tag{1}$$

Here T is the absolute temperature, $\chi = \sigma S$, with S being the Seebeck coefficient and σ being the electrical conductivity at the vanishing temperature gradient, $\kappa = \lambda_E - TS^2\sigma$ is the usual thermal conductivity at zero electric current, and λ_E is the thermal conductivity at vanishing electric field. Such an enhancement would lead to more efficient thermoelectric heat pumps and electric power generators and could revolutionize those practical applications [14]. Efficient electric power generation based upon a thermoelectric generator would enable waste heat to be utilized rather than discarded [15,16]. This would not only produce more electric power from the same available heat but would also lessen the heat pollution resulting from discarded heat.

Studies of thermoelectricity in a composite medium were often also motivated by the quest for an enhanced value of ZT and Δ. However, one of the current authors proved that this is impossible if all the constituents have the usual kind of Seebeck coupling between the local electric field and the local temperature gradient [11,17]. The effects of a magnetic field on thermoelectric response were considered only for a superlattice and a heterojunction of GaAs and GaAlAs, which are not particularly good thermoelectric materials [18]. Some exact relations are obeyed by the macroscopic moduli of a thermoelectric composite in the absence of any magnetic field. Those were first published in Refs. [19–21]. The same relations were also obtained in Ref. [11], where they were used to prove the above-mentioned rigorous result that Δ cannot be enhanced in a composite medium.

Nevertheless, a proposal for a practical improvement of the thermoelectric properties of polycrystalline Bi by the application of a **B** field was made in 2003 [14]. More recently, it has been shown experimentally that Δ of polycrystalline (and therefore isotropic) bismuth can be enhanced by the application of a **B** field or by the embedding of nanometer-sized inclusions [22]. In view of the theorem proved in Refs. [11,17], the enhancement due to the nanostructure in the absence of a **B** field can only be the result of changes in the microscopic transport properties.

When a magnetic field H is applied to a composite medium (Fig. 1 shows the slab media depicted separately in Fig. 2), the scalar effective macroscopic moduli σ_e, S_e, and κ_e in Eq. (1) become tensors, and the expression for the figure of merit [for each branch (l) or (r); see Fig. 1 and Refs. [23,24]] takes the form

$$ZT = \frac{S_{XX}^{(e)2} T}{\rho_{XX}^{(e)} \kappa_{XX}^{(e)}}. \tag{2}$$

This is the so-called longitudinal operating mode, and we have used here the uppercase subscripts X, Y, and Z in order to distinguish the coordinate system X,Y,Z, connected to the

*strelnik@mail.biu.ac.il

†bergman@post.tau.ac.il

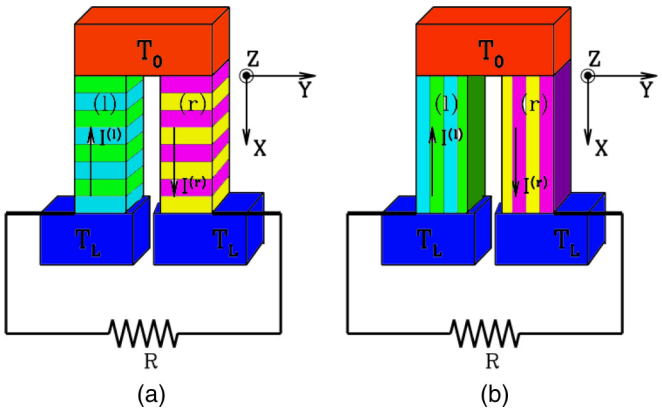

FIG. 1. Schematic drawing of the thermomagnetic device when two device arms (denoted l and r) are clamped between heat reservoirs at temperatures T_0 and T_L. The longitudinal operating mode is defined (see Refs. [23,24]) when both heat and electric current $\mathbf{I}$ flow along the X axis. The magnetic field $\mathbf{B}$ is aligned with the Z axis. When the external circuit element is a load resistor R, then this device represents a generator (in this case $T_L < T_0$). If the external circuit element is a battery, then the device is made to operate as a refrigerator (when $T_L > T_0$). (a) Situation when the slabs are perpendicular to the current $\mathbf{I}$ and X axis of the thermoelectric device. (b) Situation when the slabs are parallel to the current $\mathbf{I}$ and X axis of the thermoelectric device. The coordinate system indicated by the uppercase letters X,Y,Z is connected to thermoelectric devices and is directed as in Refs. [23,24], while everywhere else (see Figs. 2, 4) the coordinate system indicated by lower case letters x,y,z is connected to the composite microstructure (in accordance with Fig. 2 for slabs and Fig. 4 for a periodical array of spherical and/or cylindrical inclusions).

thermoelectric device (shown in Fig. 1 and in Refs. [23,24]), from the coordinate system connected to the composite microstructure shown in Fig. 4 below and characterized by the lowercase coordinate axes x,y,z.

As follows from Eq. (2), ZT depends in particular on the value of the magnetoresistivity $\rho^{(e)}_{XX}(H)$. The current authors studied the magnetoresistivity of a conducting composite where the microstructure is spatially periodic. It was found that, when the Hall to transverse Ohmic resistivity ratio, denoted by H, is greater than 1 in at least one of the constituents, then all the elements of the macroscopic resistivity tensor become strongly dependent on the precise direction of $\mathbf{B}$ with respect to the symmetry axes [25–29]. Those predictions were later verified, quantitatively, in experiments [30,31].

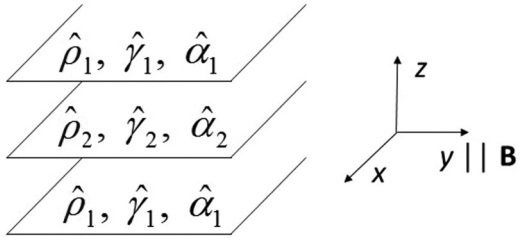

FIG. 2. Parallel-slab microstructure where the slabs are perpendicular to the z axis and a uniform magnetic field $\mathbf{B}$ is applied parallel to the slabs along the y axis.

It seems that no one has studied the behavior of a composite structure where at least one of the constituents has a strong thermoelectric response and another constituent has a strong Hall effect, i.e., $|H| > 1$.

The remainder of this paper is organized as follows. In Sec. II we write down the system of coupled equations for the local electric potential $\phi(\mathbf{r})$ and the local temperature $T(\mathbf{r})$, which follow from the conservation laws of the entropic and electric currents. We write the simple $\mathbf{B}$-dependent expressions for the local 6×6 "conductivity" tensor and the general expressions for the elements of the 6×6 macroscopic or bulk effective conductivity tensor. Using these expressions, in Sec. III we evaluate analytically the effective moduli of the 6×6 "resistivity" tensor for the microstructure of parallel slabs in the presence of an externally applied uniform magnetic field $\mathbf{B}$ which is parallel to those slabs. These predictions are verified numerically using a numerical approach developed by us and described in detail in Sec. IV. The general solution in this approach is based on a Fourier expansion in the case of composites with periodic microstructure. Numerical results for the case of a periodic array of spheres or cylinders are presented in Sec. V. These results include the magnetic-field-induced angular anisotropy of the 6×6 conductivity and resistivity effective moduli (i.e., their dependences on the direction of the applied magnetic field $\mathbf{B}$). In Sec. VI we present some preliminary calculations on the effect of an applied magnetic field on the thermoelectric figure of merit in the case of parallel slabs and in the case of composites with a periodic microstructure. In the case of a square array of parallel circular-cylinder inclusions made of $(Bi_2Te_3)_{0.2}(Sb_2Te_3)_{0.8}$ situated in a copper host, we find that ZT increases dramatically with increasing magnetic field (see Fig. 11 below). Section VII provides a summary and discussion of the main results. For convenience, some simple evaluations are presented in the Appendix.

II. GENERAL EQUATIONS

The basic galvanothermomagnetic phenomena can be described by the following concise 6×6 matrix relation between the local six-component current density $\vec{\mathcal{J}}$ and the local six-component field $\nabla\Psi$:

$$\vec{\mathcal{J}}(\mathbf{r}) = \hat{\mathcal{S}}(\mathbf{r})\cdot\nabla\Psi(\mathbf{r}) \quad \text{or} \quad \nabla\Psi(\mathbf{r}) = \hat{\mathcal{R}}(\mathbf{r})\cdot\vec{\mathcal{J}}(\mathbf{r}), \tag{3}$$

where

$$\vec{\mathcal{J}} \equiv \begin{pmatrix} -\mathbf{J} \\ -\mathbf{J}_S \end{pmatrix}, \quad \Psi \equiv \begin{pmatrix} \phi \\ T \end{pmatrix}, \tag{4}$$

$$\hat{\mathcal{S}} \equiv \begin{pmatrix} \hat{\sigma} & \hat{\chi} \\ \hat{\zeta} & \hat{\lambda} \end{pmatrix}, \quad \hat{\mathcal{R}} \equiv \hat{\mathcal{S}}^{-1} = \begin{pmatrix} \hat{\rho} & \hat{\alpha} \\ \hat{\beta} & \hat{\gamma} \end{pmatrix}. \tag{5}$$

Here $\mathbf{J}(\mathbf{r})$ and $\mathbf{J}_S(\mathbf{r})$ are the electric and entropic current densities, respectively, while $\nabla\phi$ and ∇T are the electric and temperature fields, respectively. The 6×6 conductivity $\hat{\mathcal{S}}$ and 6×6 resistivity $\hat{\mathcal{R}}$ matrices have been partitioned into four blocks, each of which contains, in general, nine entries. We will call $\hat{\rho}$, $\hat{\alpha}$, $\hat{\beta}$, and $\hat{\gamma}$ the 6×6 resistivity tensor components, while $\hat{\sigma}$, $\hat{\chi}$, $\hat{\zeta}$, and $\hat{\lambda}$ will be called the 6×6 conductivity tensor components.

Note again that in Eq. (5) $\hat{\chi} = \hat{\sigma}\hat{S}$, where S is the Seebeck coefficient. It is worth noting also that the equation for J_S in Eqs. (3)–(5) differs from the one usually used by other authors, $-\mathbf{J}_S = \hat{\zeta}\nabla\phi + (\hat{\chi}^2\hat{\sigma}^{-1} + \hat{\kappa}/T)\nabla T$. That is because we have linearized it by treating $\hat{\lambda} \equiv \hat{\chi}^2\hat{\sigma}^{-1} + \hat{\kappa}/T$ as a constant [11,32,33] (here $\hat{\kappa}$ is the thermal conductivity).

In order to understand the physical meaning of the transport coefficients which appear in $\hat{\mathcal{S}}$ (or $\hat{\mathcal{R}}$) and compare our results with other publications, we need to rewrite Eqs. (3)–(5) in the form of Refs. [16,23,34]:

$$\begin{pmatrix} -\mathbf{J}_S \\ -\nabla\phi \end{pmatrix} = \begin{pmatrix} \hat{\kappa}/T & -\hat{\Pi}/T \\ \hat{S} & \hat{\sigma}^{-1} \end{pmatrix} \begin{pmatrix} \nabla T \\ \mathbf{J} \end{pmatrix} \tag{6}$$

$$= \begin{pmatrix} \hat{\lambda} - \hat{\zeta}\hat{\sigma}^{-1}\hat{\chi} & -\hat{\zeta}\hat{\sigma}^{-1} \\ \hat{\sigma}^{-1}\hat{\chi} & \hat{\sigma}^{-1} \end{pmatrix} \begin{pmatrix} \nabla T \\ \mathbf{J} \end{pmatrix} \tag{7}$$

$$= \begin{pmatrix} \hat{\gamma}^{-1} & \hat{\gamma}^{-1}\hat{\beta} \\ -\hat{\alpha}\hat{\gamma}^{-1} & \hat{\rho} - \hat{\alpha}\hat{\gamma}^{-1}\hat{\beta} \end{pmatrix} \begin{pmatrix} \nabla T \\ \mathbf{J} \end{pmatrix}, \tag{8}$$

where $\hat{\boldsymbol{\kappa}} = T(\hat{\lambda} - \hat{\zeta}\hat{\sigma}^{-1}\hat{\chi}) = T\hat{\gamma}^{-1}$ is the thermal conductivity tensor at zero electric current, $\hat{\lambda} = \hat{\lambda}_E/T$, where $\hat{\lambda}_E$ is the thermal conductivity tensor at zero electric field, $\hat{\Pi} = T\hat{\zeta}\hat{\sigma}^{-1} = -T\hat{\gamma}^{-1}\hat{\beta}$ is the Peltier tensor, $\hat{S} = \hat{\sigma}^{-1}\hat{\chi} = -\hat{\alpha}\hat{\gamma}^{-1}$ is the Seebeck tensor, and $\hat{\sigma}^{-1} = \hat{\rho} - \hat{\alpha}\hat{\gamma}^{-1}\hat{\beta}$ is the resistivity tensor at zero temperature gradient.

From the conservation law of the six-component current

$$\nabla \cdot \vec{\mathcal{J}} = \nabla \cdot \hat{\mathcal{S}}(\mathbf{r}) \cdot \nabla\Psi = 0, \tag{9}$$

the following coupled differential equations for the local electric potential $\phi(\mathbf{r})$ and the local temperature $T(\mathbf{r})$ are obtained:

$$\nabla \cdot \hat{\sigma}(\mathbf{r}) \cdot \nabla\phi + \nabla \cdot \hat{\chi}(\mathbf{r}) \cdot \nabla T = 0, \tag{10}$$

$$\nabla \cdot \hat{\zeta}(\mathbf{r}) \cdot \nabla\phi + \nabla \cdot \hat{\lambda}(\mathbf{r}) \cdot \nabla T = 0. \tag{11}$$

Here $\hat{\sigma}(\mathbf{r})$, $\hat{\chi}(\mathbf{r})$, $\hat{\zeta}(\mathbf{r})$, and $\hat{\lambda}(\mathbf{r})$ are second-rank tensors that have different values in the different constituents.

A. Macroscopic or bulk effective moduli

The main aim of our paper is to find a macroscopic relation between the volume-averaged fields and currents. This defines the macroscopic or bulk effective moduli $\hat{\sigma}_e$, $\hat{\chi}_e$, $\hat{\zeta}_e$, and $\hat{\lambda}_e$:

$$\langle \mathbf{J} \rangle \equiv \langle \hat{\sigma}(\mathbf{r}) \cdot \nabla\phi \rangle + \langle \hat{\chi}(\mathbf{r}) \cdot \nabla T \rangle = \hat{\sigma}_e \cdot \langle \nabla\phi \rangle + \hat{\chi}_e \cdot \langle \nabla T \rangle, \tag{12}$$

$$\langle \mathbf{J}_S \rangle \equiv \langle \hat{\zeta}(\mathbf{r}) \cdot \nabla\phi \rangle + \langle \hat{\lambda}(\mathbf{r}) \cdot \nabla T \rangle = \hat{\zeta}_e \cdot \langle \nabla\phi \rangle + \hat{\lambda}_e \cdot \langle \nabla T \rangle, \tag{13}$$

where $\langle \cdots \rangle$ denotes volume averaging.

B. Local tensors

For simplicity we will assume that $\hat{\alpha}$, $\hat{\beta}$, and $\hat{\gamma}$ in Eq. (5) are diagonal scalar matrices: $\hat{\alpha} \equiv \alpha\hat{I}$, $\hat{\beta} \equiv \beta\hat{I}$, and $\hat{\gamma} \equiv \gamma\hat{I}$, where $\hat{I}$ is the 3×3 unit matrix. By contrast, in the resistivity matrix $\hat{\rho}$ all nine components can be nonzero in general. For arbitrary direction of the magnetic induction field $\mathbf{B}$ and when $\hat{\beta} = \hat{\alpha}$, Eq. (5) takes the form

$$\hat{\mathcal{R}} = \begin{pmatrix} \hat{\rho} & \hat{\alpha} \\ \hat{\alpha} & \hat{\gamma} \end{pmatrix} = \begin{pmatrix} \rho & \rho H_z & -\rho H_y & \alpha & 0 & 0 \\ -\rho H_z & \rho & \rho H_x & 0 & \alpha & 0 \\ \rho H_y & -\rho H_x & \rho & 0 & 0 & \alpha \\ \alpha & 0 & 0 & \gamma & 0 & 0 \\ 0 & \alpha & 0 & 0 & \gamma & 0 \\ 0 & 0 & \alpha & 0 & 0 & \gamma \end{pmatrix}. \tag{14}$$

The inverse of this matrix, i.e., the 6×6 conductivity tensor, then takes the form

$$\hat{\mathcal{S}} = \hat{\mathcal{R}}^{-1} = \begin{pmatrix} \hat{\rho} & \hat{\alpha} \\ \hat{\alpha} & \hat{\gamma} \end{pmatrix}^{-1} \equiv \begin{pmatrix} \hat{\sigma} & \hat{\chi} \\ \hat{\zeta} & \hat{\lambda} \end{pmatrix}, \tag{15}$$

where the four 3×3 matrix blocks of the 6×6 conductivity tensor have the form

$$\hat{\sigma} = \frac{1}{\xi[\xi^2 + \gamma^2\rho^2 H^2]} \begin{pmatrix} -\gamma\left[\xi^2 + \gamma^2\rho^2 H_x^2\right] & -\gamma^2\rho[\xi H_z + \gamma\rho H_x H_y] & \gamma^2\rho[\xi H_y - \gamma\rho H_x H_z] \\ \gamma^2\rho[\xi H_z - \gamma\rho H_x H_y] & -\gamma\left[\xi^2 + \gamma^2\rho^2 H_y^2\right] & -\gamma^2\rho[\xi H_x + \gamma\rho H_y H_z] \\ -\gamma^2\rho[\xi H_y + \gamma\rho H_x H_z] & \gamma^2\rho[\xi H_x - \gamma\rho H_y H_z] & -\gamma\left[\xi^2 + \gamma^2\rho^2 H_z^2\right] \end{pmatrix}, \tag{16}$$

$$\hat{\chi} = \hat{\zeta} = -\frac{\alpha}{\gamma}\hat{\sigma}, \quad \hat{\lambda} = \frac{\alpha^2}{\gamma^2}\hat{\sigma} + \frac{1}{\gamma}\hat{I}, \tag{17}$$

where $\xi \equiv \alpha^2 - \gamma\rho < 0$ (since $\hat{\mathcal{R}}$ is a positive-definite matrix) and $\hat{I}$ is the unit matrix.

In the local 6×6 resistivity and conductivity tensors in Eq. (15) we have assumed that $\hat{\beta} = \hat{\alpha}$ and $\hat{\zeta} = \hat{\chi}$. However, the effective values of these tensors are not necessarily equal in the presence of the magnetic field $\mathbf{B}$. In the presence of such a field the macroscopic Seebeck matrices will usually acquire some off-diagonal elements that are odd functions of the constituent Hall resistivities and therefore change sign between the upper right block and the lower left block of the 6×6 matrix of macroscopic transport coefficients, as we shall see below.

III. PARALLEL SLABS: THEORETICAL PREDICTIONS

In a simple two-constituent flat slabs microstructure (see Fig. 2) it is possible to calculate the local electric field $\nabla\phi$ and temperature gradient ∇T, as well as the macroscopic

response, in closed form. This is achieved using elementary but somewhat complicated linear algebra.

We assumed, for simplicity, that all the constituents exhibit isotropic response, that the slabs are all perpendicular to the z-axis, and that a uniform magnetic field $\mathbf{B}$ is applied along the y axis (see Fig. 2). Then in Eq. (14) only two off-diagonal terms ($\rho_{xz} = -\rho H_y$ and $\rho_{zx} = \rho H_y$ which we define below as $-\rho_H$ and ρ_H, respectively) are nonzero. Direct volume averaging in Eqs. (12)-(13) leads then after straightforward algebra to the following analytical expressions for the elements of the various 3×3 blocks in that 6×6 matrix:

$$\rho_{xx}^{(e)} = \rho_{yy}^{(e)} = D^{-1}\left\langle \frac{\rho}{\rho\gamma - \alpha^2} \right\rangle, \tag{18}$$

$$\rho_{zz}^{(e)} = \langle \rho \rangle + \left\langle \frac{\gamma \rho_H^2}{\rho\gamma - \alpha^2} \right\rangle + D^{-1}\left[2\left\langle \frac{\gamma\rho_H}{\rho\gamma - \alpha^2} \right\rangle \left\langle \frac{\alpha\rho_H}{\rho\gamma - \alpha^2} \right\rangle \left\langle \frac{\alpha}{\rho\gamma - \alpha^2} \right\rangle - \left\langle \frac{\alpha\rho_H}{\rho\gamma - \alpha^2} \right\rangle^2 \left\langle \frac{\gamma}{\rho\gamma - \alpha^2} \right\rangle - \left\langle \frac{\gamma\rho_H}{\rho\gamma - \alpha^2} \right\rangle^2 \left\langle \frac{\rho}{\rho\gamma - \alpha^2} \right\rangle \right], \tag{19}$$

$$\rho_{zx}^{(e)} = -\rho_{xz}^{(e)} = D^{-1}\left[\left\langle \frac{\alpha\rho_H}{\rho\gamma - \alpha^2} \right\rangle \left\langle \frac{\alpha}{\rho\gamma - \alpha^2} \right\rangle - \left\langle \frac{\gamma\rho_H}{\rho\gamma - \alpha^2} \right\rangle \left\langle \frac{\rho}{\rho\gamma - \alpha^2} \right\rangle \right], \tag{20}$$

$$\gamma_{xx}^{(e)} = \gamma_{yy}^{(e)} = D^{-1}\left\langle \frac{\gamma}{\rho\gamma - \alpha^2} \right\rangle, \tag{21}$$

$$\gamma_{zz}^{(e)} = \langle \gamma \rangle \tag{22}$$

$$\alpha_{xx}^{(e)} = \alpha_{yy}^{(e)} = \beta_{xx}^{(e)} = \beta_{yy}^{(e)} = D^{-1}\left\langle \frac{\alpha}{\rho\gamma - \alpha^2} \right\rangle, \quad \alpha_{zz}^{(e)} = \beta_{zz}^{(e)} = \langle \alpha \rangle, \tag{23}$$

$$\alpha_{zx}^{(e)} = -\beta_{xz}^{(e)} = D^{-1}\left[\left\langle \frac{\alpha\rho_H}{\rho\gamma - \alpha^2} \right\rangle \left\langle \frac{\gamma}{\rho\gamma - \alpha^2} \right\rangle - \left\langle \frac{\gamma\rho_H}{\rho\gamma - \alpha^2} \right\rangle \left\langle \frac{\alpha}{\rho\gamma - \alpha^2} \right\rangle \right], \tag{24}$$

$$D \equiv \left\langle \frac{\rho}{\rho\gamma - \alpha^2} \right\rangle \left\langle \frac{\gamma}{\rho\gamma - \alpha^2} \right\rangle - \left\langle \frac{\alpha}{\rho\gamma - \alpha^2} \right\rangle^2, \tag{25}$$

where $\langle \ldots \rangle$ denotes, as previously, the volume average. All the other matrix elements vanish. Note that when we set $\alpha_1 = \alpha_2 = 0$ these results reduce to what we would expect to get when there is no interaction between the electric and thermal transport processes. In particular, $\hat{\rho}^{(e)}$ depends only on the constituent electric resistivities while $\hat{\gamma}^{(e)}$ is a scalar and depends only on the constituent thermal resistivities.

We have applied the numerical scheme described in Sec. IV to the same parallel slabs microstructure. The two sets of results are in excellent agreement, as is evident from Fig. 3, where all 16 elements of the macroscopic 6×6 resistivity tensor are plotted vs. the dimensionless magnetic field H_2 of constituent 2.

Some numerical results based on the closed form expressions listed above are plotted in Fig. 3. In particular, the longitudinal thermoelectric figure of merit ZT (that is when the macroscopic electric and thermal currents flow along parallel directions) which arises from these results is plotted in Figs. 3(q) and 3(r). They are certainly not good for any practical application, since in one case ZT is independent of H and in the other case it decreases with increasing H.

IV. GENERAL SOLUTION AND NUMERICAL SCHEME

As in Sec. III, we consider a two-constituent composite but with a general microstructure. It is convenient to represent the coordinate dependence of the various local moduli tensors with the help of the characteristic step function $\theta_1(\mathbf{r})$, e.g.,

$$\hat{\sigma}(\mathbf{r}) = \hat{\sigma}_1\theta_1(\mathbf{r}) + \hat{\sigma}_2\theta_2(\mathbf{r}) = \hat{\sigma}_2 - \delta\hat{\sigma}\theta_1(\mathbf{r}), \tag{26}$$

where $\theta_i(\mathbf{r}) = 1$ if $\mathbf{r}$ is in constituent i but vanishes elsewhere and where $\delta\hat{\sigma} \equiv \hat{\sigma}_2 - \hat{\sigma}_1$. The local thermal conductivities $\hat{\lambda}_i(\mathbf{r})$ and Seebeck coefficients $\hat{\chi}_i(\mathbf{r})$, $\hat{\zeta}_i(\mathbf{r})$ can be represented in a similar fashion with $\delta\hat{\chi} \equiv \hat{\chi}_2 - \hat{\chi}_1$, $\delta\hat{\zeta} \equiv \hat{\zeta}_2 - \hat{\zeta}_1$, $\delta\hat{\lambda} \equiv \hat{\lambda}_2 - \hat{\lambda}_1$. Equations (10) and (11) can then be rewritten as

$$\nabla \cdot \hat{\sigma}_2 \cdot \nabla\phi = -\nabla \cdot \hat{\chi}_2 \cdot \nabla T + \nabla \cdot \delta\hat{\sigma}\theta_1(\mathbf{r}) \cdot \nabla\phi + \nabla \cdot \delta\hat{\chi}\theta_1 \cdot \nabla T, \tag{27}$$

$$\nabla \cdot \hat{\lambda}_2 \cdot \nabla T = -\nabla \cdot \hat{\zeta}_2 \cdot \nabla\phi + \nabla \cdot \delta\hat{\zeta}\theta_1(\mathbf{r}) \cdot \nabla\phi + \nabla \cdot \delta\hat{\lambda}\theta_1 \cdot \nabla T. \tag{28}$$

The Green's functions in Eqs. (27) and (28) are defined by

$$\nabla \cdot \hat{\sigma}_2 \cdot \nabla G_\sigma(\mathbf{r} - \mathbf{r}') = -\delta^3(\mathbf{r} - \mathbf{r}'), \tag{29}$$

$$\nabla \cdot \hat{\lambda}_2 \cdot \nabla G_\lambda(\mathbf{r} - \mathbf{r}') = -\delta^3(\mathbf{r} - \mathbf{r}'), \tag{30}$$

with $G_\sigma = 0$ and $G_\lambda = 0$ at the system boundaries. Using these Green's functions, Eqs. (27) and (28) can be transformed into a pair of coupled integro-differential equations:

$$\psi \equiv \phi - \phi_0 = \int dV' \theta_1' \nabla' G_\sigma \cdot \delta\hat{\sigma} \cdot \nabla'(\psi' + \phi_0) + \int dV' \theta_1' \nabla' G_\sigma \cdot \delta\hat{\chi} \cdot \nabla'(\tau + T_0) - \int dV' \nabla' G_\sigma \cdot \hat{\chi}_2 \cdot \nabla'(\tau + T_0), \tag{31}$$

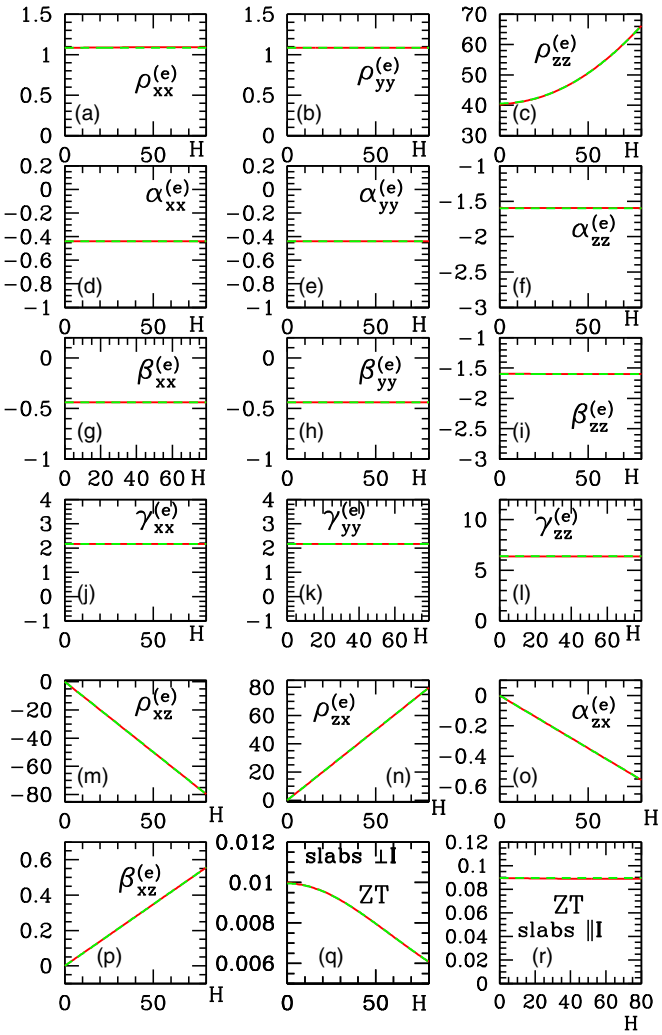

FIG. 3. (a)–(p) Macroscopic or bulk effective values of all 16 nonzero elements of the 6×6 resistivity tensor components of a simple two-constituent flat-slab microstructure (see Fig. 2) vs the dimensionless magnetic field $H_2 \equiv H$. Green dashed lines show the theoretical predictions (18)–(25) (see Sec. III). Solid red lines show numerical calculations (using the numerical scheme described in Secs. II–IV) of a periodic array of parallel slabs with a total thickness of constituent 1 of $h = 0.4a$ (a is the total thickness of the composite). The following constituent parameters were used: $\rho_2 = 1$, $\gamma_2 = 10$, $\alpha_2 = -2$, $\rho_1 = 100$, $\gamma_1 = 1$, $\alpha_1 = -1$, $H_1 = 0$ (all in arbitrary units). The magnetic field $\mathbf{B}$ is parallel to the y axis. (q) and (r) Figure of merit ZT vs H of the same system of flat parallel slabs when the macroscopic currents are perpendicular and parallel to the slabs, respectively.

$$\tau \equiv T - T_0 = \int dV' \theta_1' \nabla' G_\lambda \cdot \delta\hat{\lambda} \cdot \nabla'(\tau + T_0) + \int dV' \theta_1' \nabla' G_\lambda \cdot \delta\hat{\zeta} \cdot \nabla'(\psi' + \phi_0) - \int dV' \nabla' G_\lambda \cdot \hat{\zeta}_2 \cdot \nabla'(\psi' + \phi_0), \quad (32)$$

where the primes denote that the argument or variable is $\mathbf{r}'$, $\psi \equiv \phi - \phi_0$, and $\tau \equiv T - T_0$ are the distorted parts of ϕ and T and where we have performed integration by parts.

We now assume that $T_0(\mathbf{r})$ and $\phi_0(\mathbf{r})$ are linear functions of $\mathbf{r}$. Therefore ∇T_0 and $\nabla\phi_0$ are constants, and $\nabla \cdot \hat{\alpha}_2 \cdot \nabla T_0 = \nabla \cdot \hat{\beta}_2 \cdot \nabla\phi_0 = \nabla \cdot \hat{\sigma}_2 \cdot \nabla\phi_0 = \nabla \cdot \hat{\gamma}_2 \cdot \nabla T_0 = 0$. Equations (31) and (32) then become

$$\psi = \int dV' \theta_1' [\nabla' G_\sigma \cdot \delta\hat{\sigma} \cdot (\nabla'\phi_0' + \nabla'\psi') + \nabla' G_\sigma \cdot \delta\hat{\chi} \cdot (\nabla' T_0' + \nabla'\tau')] - \int dV' \nabla' G_\sigma \cdot \hat{\chi}_2 \cdot \nabla'\tau', \quad (33)$$

$$\tau = \int dV' \theta_1' [\nabla' G_\lambda \cdot \delta\hat{\lambda} \cdot (\nabla' T_0' + \nabla'\tau') + \nabla' G_\lambda \cdot \delta\hat{\zeta} \cdot (\nabla'\phi_0' + \nabla'\psi')] - \int dV' \nabla' G_\lambda \cdot \hat{\zeta}_2 \cdot \nabla'\psi'. \quad (34)$$

These are two coupled integro-differential equations for $\psi(\mathbf{r})$ and $\tau(\mathbf{r})$.

A. Periodic composite: Fourier expansion

When the composite medium has a periodic microstructure, great simplifications ensue due to the fact that $\theta_1(\mathbf{r})$ is now a periodic function [25,26,35]. From the fact that, away from the external boundaries, G_σ and G_λ depend on $\mathbf{r}$ and $\mathbf{r}'$ only through their differences $\mathbf{r} - \mathbf{r}'$, we get that $\psi(\mathbf{r})$ and $\tau(\mathbf{r})$ are periodic and therefore can be expanded in Fourier series:

$$\psi(\mathbf{r}) = \sum_{\mathbf{g}} \psi_{\mathbf{g}} e^{i\mathbf{g}\cdot\mathbf{r}}, \quad \tau(\mathbf{r}) = \sum_{\mathbf{g}} \tau_{\mathbf{g}} e^{i\mathbf{g}\cdot\mathbf{r}}, \quad (35)$$

where the sums are over all the vectors $\mathbf{g}$ of the appropriate reciprocal lattice. The Fourier expansion coefficient of an arbitrary periodic function $f(\mathbf{r})$ is given by

$$f_{\mathbf{g}} = \frac{1}{V_a} \int_{V_a} dV e^{-i\mathbf{g}\cdot\mathbf{r}} f(\mathbf{r}). \quad (36)$$

The Fourier transforms of G_σ and G_λ [see Eqs. (29) and (30)] which vanish at infinity have simple forms, namely,

$$\int dV e^{-i\mathbf{k}\cdot(\mathbf{r}-\mathbf{r}')} G_\sigma(\mathbf{r},\mathbf{r}') = \frac{1}{\mathbf{k} \cdot \hat{\sigma}_2 \cdot \mathbf{k}}, \quad (37)$$

$$\int dV e^{-i\mathbf{k}\cdot(\mathbf{r}-\mathbf{r}')} G_\lambda(\mathbf{r},\mathbf{r}') = \frac{1}{\mathbf{k} \cdot \hat{\lambda}_2 \cdot \mathbf{k}}, \quad (38)$$

which depend only on the symmetric parts of $\hat{\sigma}_2$ and $\hat{\lambda}_2$.

We now expand the periodic functions $\tau(\mathbf{r})$, $\psi(\mathbf{r})$, and $\theta_1(\mathbf{r})$ in Fourier series, as in Eq. (35), and express $G_\sigma(\mathbf{r},\mathbf{r}')$ and $G_\lambda(\mathbf{r},\mathbf{r}')$ as Fourier integrals. We then define

$$a_{\mathbf{g}} \equiv i|\mathbf{g}|(\mathbf{e}_{\mathbf{g}} \cdot \hat{\sigma}_2 \cdot \mathbf{e}_{\mathbf{g}})\psi_{\mathbf{g}}, \quad b_{\mathbf{g}} \equiv i|\mathbf{g}|(\mathbf{e}_{\mathbf{g}} \cdot \hat{\lambda}_2 \cdot \mathbf{e}_{\mathbf{g}})\tau_{\mathbf{g}}, \quad (39)$$

where $\mathbf{e}_{\mathbf{g}} \equiv \mathbf{g}/|\mathbf{g}|$ is the unit vector along $\mathbf{g}$. Equations (33) and (34) now translate into the following set of linear algebraic

equations for the modified Fourier coefficients $a_{\mathbf{g}}$ and $b_{\mathbf{g}}$:

$$a_{\mathbf{g}} + \frac{(\mathbf{e_g}\cdot\hat{\chi}_2\cdot\mathbf{e_g})}{(\mathbf{e_g}\cdot\hat{\lambda}_2\cdot\mathbf{e_g})}b_{\mathbf{g}} = \theta_{\mathbf{g}}[(\mathbf{e_g}\cdot\delta\hat{\sigma}\cdot\nabla\phi_0)+(\mathbf{e_g}\cdot\delta\hat{\chi}\cdot\nabla T_0)] + \sum_{\mathbf{g}'}\theta_{\mathbf{g}-\mathbf{g}'}\left[\frac{(\mathbf{e_g}\cdot\delta\hat{\sigma}\cdot\mathbf{e_{g'}})}{(\mathbf{e_{g'}}\cdot\hat{\sigma}_2\cdot\mathbf{e_{g'}})}a_{\mathbf{g}'} + \frac{(\mathbf{e_g}\cdot\delta\hat{\chi}\cdot\mathbf{e_{g'}})}{(\mathbf{e_{g'}}\cdot\hat{\lambda}_2\cdot\mathbf{e_{g'}})}b_{\mathbf{g}'}\right], \tag{40}$$

$$b_{\mathbf{g}} + \frac{(\mathbf{e_g}\cdot\hat{\xi}_2\cdot\mathbf{e_g})}{(\mathbf{e_g}\cdot\hat{\sigma}_2\cdot\mathbf{e_g})}a_{\mathbf{g}} = \theta_{\mathbf{g}}[(\mathbf{e_g}\cdot\delta\hat{\lambda}\cdot\nabla T_0)+(\mathbf{e_g}\cdot\delta\hat{\xi}\cdot\nabla\phi_0)] + \sum_{\mathbf{g}'}\theta_{\mathbf{g}-\mathbf{g}'}\left[\frac{(\mathbf{e_g}\cdot\delta\hat{\lambda}\cdot\mathbf{e_{g'}})}{(\mathbf{e_{g'}}\cdot\hat{\lambda}_2\cdot\mathbf{e_{g'}})}b_{\mathbf{g}'} + \frac{(\mathbf{e_g}\cdot\delta\hat{\xi}\cdot\mathbf{e_{g'}})}{(\mathbf{e_{g'}}\cdot\hat{\sigma}_2\cdot\mathbf{e_{g'}})}a_{\mathbf{g}'}\right]. \tag{41}$$

These equations will be solved for nonzero $\mathbf{g}$ either by direct numerical solution of a finite subset or by a variety of series expansion procedures as described in Ref. [26]. The coefficients $a_{\mathbf{g}=0}$ and $b_{\mathbf{g}=0}$ both vanish. However, the Fourier coefficients $\psi_{\mathbf{g}=0}$ and $\tau_{\mathbf{g}=0}$ are irrelevant when calculating the fields $\nabla\psi$ and ∇T.

B. Macroscopic values of the 3 × 3 tensors $\hat{\sigma}_e$, $\hat{\chi}_e$, $\hat{\xi}_e$, and $\hat{\lambda}_e$

It is convenient to solve Eqs. (40) and (41) first for the case where $\nabla\phi_0 = \mathbf{e}_\eta$ and $\nabla T_0 = 0$ and then for the case where $\nabla T_0 = \mathbf{e}_\eta$ and $\nabla\phi_0 = 0$. We will denote these solutions, respectively, by $a_{\mathbf{g}}(\nabla\phi_0)$, $b_{\mathbf{g}}(\nabla\phi_0)$ and $a_{\mathbf{g}}(\nabla T_0)$, $b_{\mathbf{g}}(\nabla T_0)$. From Eqs. (12) and (13) we then get

$$(\hat{\sigma}_2 - \hat{\sigma}_e - p_1\delta\hat{\sigma})_{\xi\eta} = \sum_{\mathbf{g}}\theta_{-\mathbf{g}}\frac{(\mathbf{e}_\xi\cdot\delta\hat{\sigma}\cdot\mathbf{e_g})}{(\mathbf{e_g}\cdot\hat{\sigma}_2\cdot\mathbf{e_g})}a_{\mathbf{g}}(\nabla\phi_0) + \sum_{\mathbf{g}}\theta_{-\mathbf{g}}\frac{(\mathbf{e}_\xi\cdot\delta\hat{\chi}\cdot\mathbf{e_g})}{(\mathbf{e_g}\cdot\hat{\lambda}_2\cdot\mathbf{e_g})}b_{\mathbf{g}}(\nabla\phi_0), \tag{42}$$

$$(\hat{\chi}_2 - \hat{\chi}_e - p_1\delta\hat{\chi})_{\xi\eta} = \sum_{\mathbf{g}}\theta_{-\mathbf{g}}\frac{(\mathbf{e}_\xi\cdot\delta\hat{\sigma}\cdot\mathbf{e_g})}{(\mathbf{e_g}\cdot\hat{\sigma}_2\cdot\mathbf{e_g})}a_{\mathbf{g}}(\nabla T_0) + \sum_{\mathbf{g}}\theta_{-\mathbf{g}}\frac{(\mathbf{e}_\xi\cdot\delta\hat{\chi}\cdot\mathbf{e_g})}{(\mathbf{e_g}\cdot\hat{\lambda}_2\cdot\mathbf{e_g})}b_{\mathbf{g}}(\nabla T_0), \tag{43}$$

$$(\hat{\zeta}_2 - \hat{\zeta}_e - p_1\delta\hat{\zeta})_{\xi\eta} = \sum_{\mathbf{g}}\theta_{-\mathbf{g}}\frac{(\mathbf{e}_\xi\cdot\delta\hat{\zeta}\cdot\mathbf{e_g})}{(\mathbf{e_g}\cdot\hat{\sigma}_2\cdot\mathbf{e_g})}a_{\mathbf{g}}(\nabla\phi_0) + \sum_{\mathbf{g}}\theta_{-\mathbf{g}}\frac{(\mathbf{e}_\xi\cdot\delta\hat{\lambda}\cdot\mathbf{e_g})}{(\mathbf{e_g}\cdot\hat{\lambda}_2\cdot\mathbf{e_g})}b_{\mathbf{g}}(\nabla\phi_0), \tag{44}$$

$$(\hat{\lambda}_2 - \hat{\lambda}_e - p_1\delta\hat{\lambda})_{\xi\eta} = \sum_{\mathbf{g}}\theta_{-\mathbf{g}}\frac{(\mathbf{e}_\xi\cdot\delta\hat{\zeta}\cdot\mathbf{e_g})}{(\mathbf{e_g}\cdot\hat{\sigma}_2\cdot\mathbf{e_g})}a_{\mathbf{g}}(\nabla T_0) + \sum_{\mathbf{g}}\theta_{-\mathbf{g}}\frac{(\mathbf{e}_\xi\cdot\delta\hat{\lambda}\cdot\mathbf{e_g})}{(\mathbf{e_g}\cdot\hat{\lambda}_2\cdot\mathbf{e_g})}b_{\mathbf{g}}(\nabla T_0). \tag{45}$$

Most of the coefficients in Eqs. (40)–(45) always remain bounded. The exceptions are the Fourier components of the characteristic function $\theta(\mathbf{r})$, namely, $\theta_{\mathbf{g}}$, which always decrease to zero when $|\mathbf{g}|$ becomes much greater than $1/a$, where a is the typical length scale of the σ_1 regions in a unit cell. For this reason Eqs. (40) and (41) for such large $\mathbf{g}$ can always be ignored in numerical calculations. A similar property holds for Eqs. (42)–(45).

V. NUMERICAL RESULTS

We have studied numerically the magnetothermoelectric response of a two-constituent composite with a periodic microstructure. This has been done for a case of three-dimensional periodicity [see Fig. 4(a)] and for the case of a columnar microstructure with two-dimensional periodicity in the perpendicular plane [see Fig. 4(b)]. In order to implement this study we have used the numerical scheme discussed in Sec. IV A. Using these computations, we have found that, like the macroscopic magnetoresistivity tensor, the thermoelectric response strongly depends on the direction of the magnetic field $\mathbf{B}$ when $|H| > 1$.

We consider two microstructures: A simple cubic array of spheres and a square array of circular cylinders. Figure 4 shows these structures and also defines a fixed coordinate system x,y,z and another coordinate system x',y,z' that rotates with the magnetic field $\mathbf{B}$, which always lies along the z' axis. Figure 4 also defines the diagonal components $\tilde{\rho}_\perp^{(e)}$, $\rho_\perp^{(e)}$, $\rho_\parallel^{(e)}$, $\tilde{\alpha}_\perp^{(e)}$, $\alpha_\perp^{(e)}$, $\alpha_\parallel^{(e)}$, etc., of the 6×6 macroscopic tensors $\hat{\mathcal{R}}_e$ and $\hat{\mathcal{S}}_e$. In Figs. 5–8 we show polar plots of some of the diagonal components of these macroscopic tensors. The constituent parameters used in these calculations were (the index 2 denotes the host medium, while the index 1 denotes the inclusions) $\rho_2 = 1.7\times 10^{-8}\ \Omega\,\mathrm{m}$, $\gamma_2 = 0.76\,\mathrm{mK^2/W}$, $\alpha_2 =$

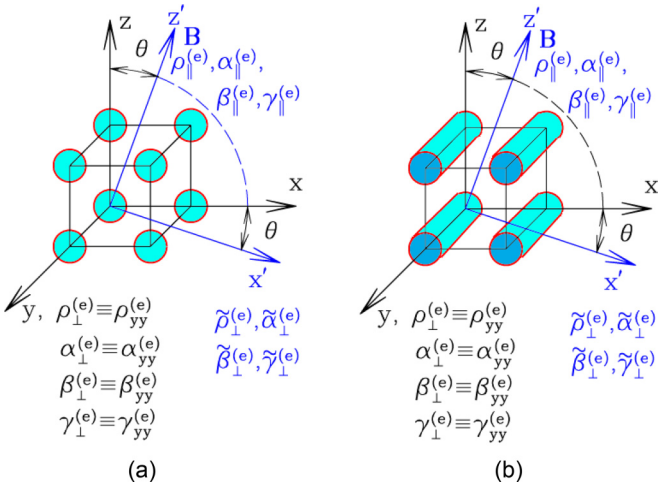

FIG. 4. Schematic drawing of the composite with periodic arrangement of (a) spheres and (b) cylinders. x,y,z is the *fixed* coordinate system, while x',y,z' is the rotating (around the y axis) coordinate system. The magnetic field $\mathbf{B}$ is directed along z' axes. The diagonal resistivity tensor components are defined as follows: $\rho_\parallel^{(e)} \equiv \rho_{z'z'}^{(e)}$, $\rho_\perp^{(e)} \equiv \rho_{yy}^{(e)} = \rho_{y'y'}^{(e)}$, $\tilde{\rho}_\perp^{(e)} = \tilde{\rho}_{x'x'}^{(e)}$. The diagonal components of $\chi^{(e)}$, $\zeta^{(e)}$, and $\gamma^{(e)}$ are defined similarly.

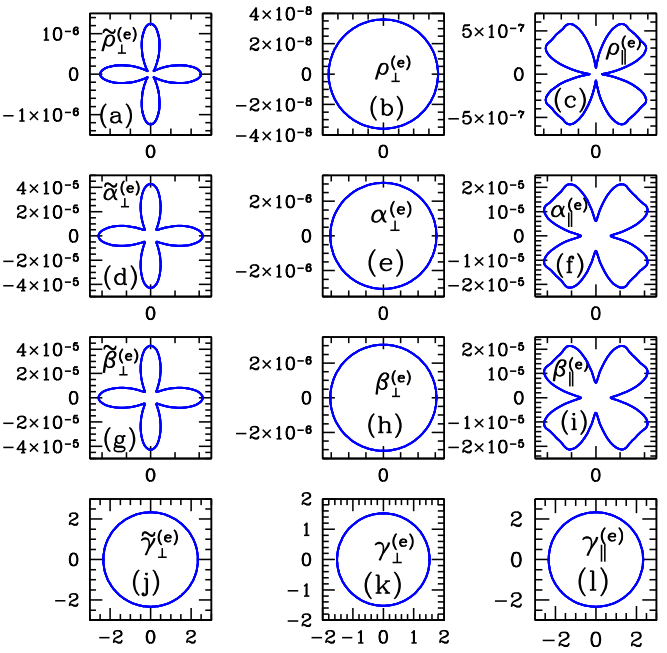

FIG. 5. Polar plots of the macroscopic or bulk effective values of the diagonal 6×6 resistivity tensor components of a periodic array of cylinders [see Fig. 4(a)] with radii $R = 0.4a$ (where a is the period of the composite) in the rotating coordinate system. The 6×6 local tensor was taken in the form of Eqs. (16) and (17) with the following ρ, α, β, and γ local parameters: For the host $\rho_2 = 1.7 \times 10^{-8}\,\Omega\,\mathrm{m}$, $\gamma_2 = 0.76\,\mathrm{mK^2/W}$, $\alpha_2 = \beta_2 = -1.4 \times 10^{-6}\,\Omega\,\mathrm{mK/V}$. These are the values for copper. For the inclusions $\rho_1 = 5 \times 10^{-5}\,\Omega\,\mathrm{m}$, $\gamma_1 = 3.7 \times 10^2\,\mathrm{mK^2/W}$, $\alpha_1 = \beta_1 = -9.25 \times 10^{-2}\,\Omega\,\mathrm{mK/V}$. These are the values for $(Bi_2Te_3)_{0.2}(Sb_2Te_3)_{0.8}$. Note that $\xi = \alpha^2 - \gamma\rho < 0$ in both the host and inclusions. The magnetic field $\mathbf{B}$ is rotating in the x,z plane [see Figs. 4(a) and 4(b)] with $H_2 = 10$ and $H_1 = 0$.

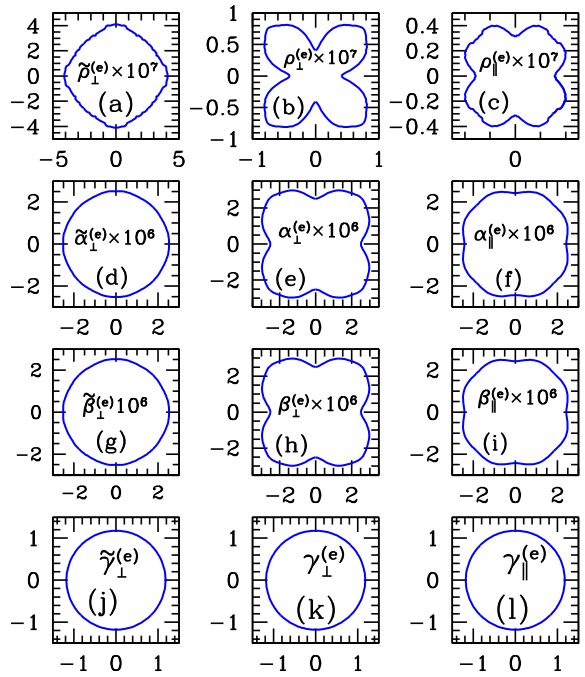

FIG. 6. Polar plots of $\hat{\rho}_e \times 10^7$, $\hat{\alpha}_e \times 10^6$, $\hat{\beta}_e \times 10^6$, and $\hat{\gamma}_e$, similar to Fig. 5, with the same values of the magnetic field and the other parameters, but for the case of a periodic cubic array of spheres (with radii $R = 0.4a$).

$\beta_2 = -1.4 \times 10^{-6}\,\Omega\mathrm{mK/V}$ (these are characteristic values for metallic copper) and $\rho_1 = 5 \times 10^{-5}\,\Omega\,\mathrm{m}$, $\gamma_1 = 3.7 \times 10^2\,\mathrm{mK^2/W}$, $\alpha_1 = \beta_1 = -9.25 \times 10^{-2}\,\Omega\mathrm{mK/V}$ [these are characteristic values for the thermoelectric metallic alloy $(Bi_2Te_3)_{0.2}(Sb_2Te_3)_{0.8}$].

From Figs. 5–7 it is evident that the diagonal components of $\hat{\rho}_e$, $\hat{\sigma}_e$, $\hat{\alpha}_e$, $\hat{\beta}_e$, $\hat{\chi}_e$, and $\hat{\zeta}_e$ strongly depend on the direction of the applied magnetic field $\mathbf{B}$. However, the diagonal components of $\hat{\gamma}_e$ are almost isotropic for the assumed values of the thermoelectric parameters of the two constituents.

The angular anisotropy of the macroscopic magnetothermoelectric tensors found in this paper looks very similar to the galvanothermoelectric and magnetoresistance anisotropy observed in some single crystals of metallic bismuth (see Fig. 9 and Refs. [2,36]) and explained using quantum mechanics [2,36–38]. By contrast, the discussion here and in Refs. [25–28,30,31] is entirely classical.

Off-diagonal 6 × 6 resistivity and conductivity tensor components

In Fig. 10 we show polar plots of the macroscopic values of the *off-diagonal* 6×6 resistivity tensor components of the periodic array of *cylinders* in the *rotating* coordinate system. In Fig. 10 only the absolute values are plotted. From the actual values that we calculated, the following relations seem to be evident:

$$\alpha_{xy}^{(e)}(H) = -\beta_{yx}^{(e)}(H), \tag{46}$$

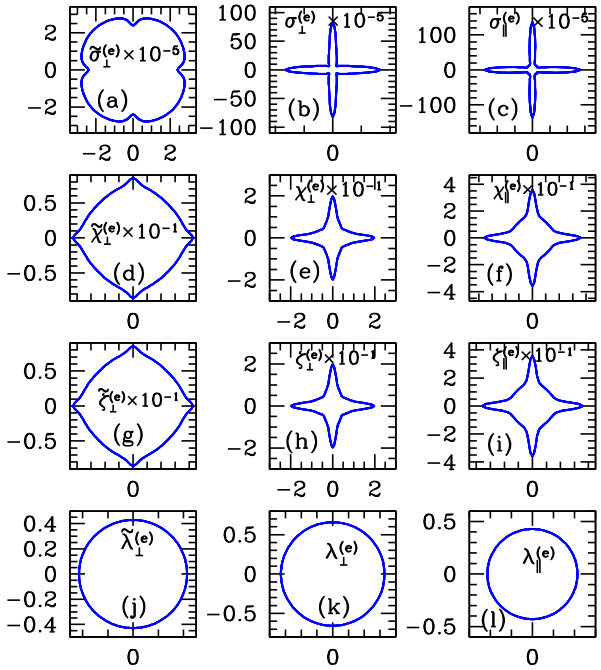

FIG. 7. Similar to Fig. 5, but for the 6×6 conductivity tensor components $\hat{\sigma}_e \times 10^{-5}$, $\hat{\chi}_e \times 10^{-2}$, $\hat{\zeta}_e \times 10^{-2}$, and $\hat{\lambda}_e$. The physical parameters and microstructure are the same as in Fig. 5.

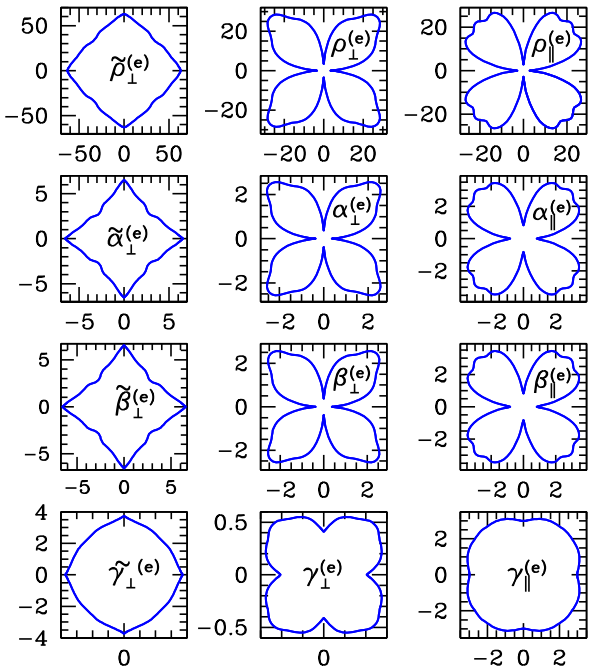

FIG. 8. Similar to Fig. 5, but for different constituent parameters: $\rho_2 = 1$, $\gamma_2 = 10$, $\alpha_2 = 2$, $\rho_1 = 100$, $\gamma_1 = 1$, and $\alpha_1 = 9$ (all in arbitrary units).

$$\alpha^{(e)}_{yz}(H) = -\beta^{(e)}_{zy}(H), \tag{47}$$

$$\alpha^{(e)}_{xz}(H) = \beta^{(e)}_{zx}(H). \tag{48}$$

Some of these and also other equalities are indicated in Fig. 10 by red arrows. These equalities are consistent with the generalized Onsager-Casimir reciprocity relations [39–41]. They will be discussed in detail in a future publication.

VI. THERMOELECTRIC FIGURE OF MERIT

The proper expressions for $S^{(e)}_{XX}$, $\rho^{(e)}_{XX}$, and $\kappa^{(e)}_{XX}$ in Eq. (2) are easily found from Eqs. (6)–(8), leading to

$$ZT = \frac{\left(\hat{\alpha}^{(e)}\hat{\gamma}_e^{-1}\right)^2_{XX}}{\left(\hat{\rho}^{(e)} - \hat{\alpha}^{(e)}\hat{\gamma}_e^{-1}\hat{\beta}^{(e)}\right)_{XX}\hat{\gamma}^{-1}_{e,XX}}. \tag{49}$$

Let the system shown in Fig. 2 be oriented so that the slabs are *perpendicular to the macroscopic electric current* $\mathbf{I}$ [see Fig. 1(a)]. We found that in this case the figure of merit ZT decreases with increasing H [see Fig. 3(q)]. In order to increase ZT with H one should consider such a composite where the magnetoresistance is negative (see Ref. [42]).

When the parallel slabs are oriented *parallel to the macroscopic current* $\mathbf{I} \parallel X$ [see Fig. 1(b)], all the macroscopic moduli that appear in the last equation do not change with H (see Fig. 3); therefore the figure of merit ZT also does not change with H [see Fig. 3(r)].

We have also performed some preliminary studies of the effect of a magnetic field H on the figure of merit ZT in the case of a *periodic array of cylinders*. We found that ZT strongly depends on the type of composite microstructure as well as on the direction of the magnetic field. In some

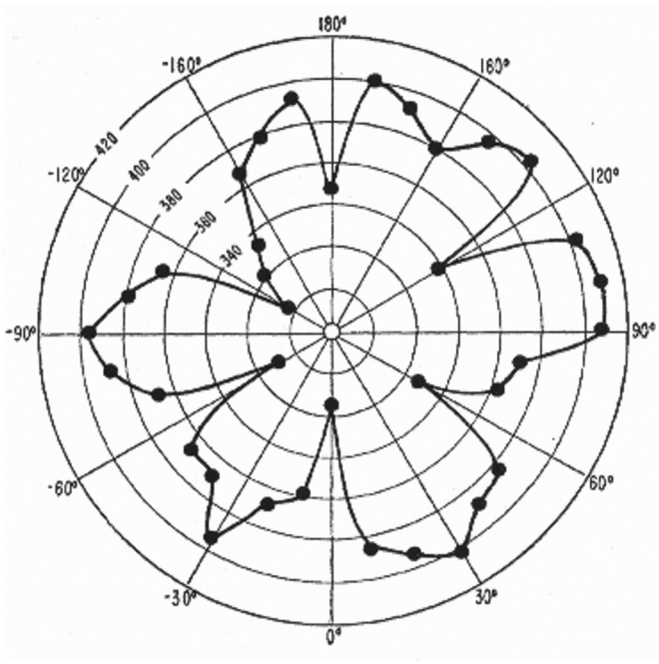

FIG. 9. Experimental polar plot of thermoelectric voltage (microvolts) as a function of magnet angle for a bismuth single crystal, $H = 12\,600$ G; the mean temperature is 5.298 K, and the temperature difference is 0.128 K. H is perpendicular to a binary axis when the magnet angle is 0°. H is perpendicular to the trigonal axis throughout the rotation. (After Ref. [2].)

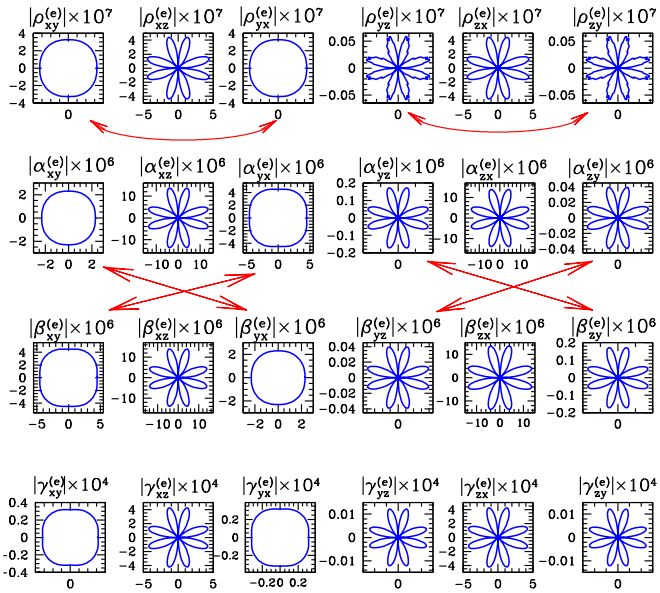

FIG. 10. Polar plots of the macroscopic or bulk effective values of the off-diagonal 6×6 resistivity tensor components ($\hat{\rho}_e \times 10^7$, $\hat{\chi}_e \times 10^6$, $\hat{\xi}_e \times 10^6$, $\hat{\lambda}_e \times 10^4$) of the same composite as in Fig. 5, with the same physical parameters, in the rotating coordinate system. Only the absolute values are plotted here. However, from the numerically calculated results it follows that $\rho^{(e)}_{xy} = -\rho^{(e)}_{yx}$, $\rho^{(e)}_{yz} = -\rho^{(e)}_{zy}$, $\rho^{(e)}_{xz} = \rho^{(e)}_{zx}$, $\gamma^{(e)}_{xy} = -\gamma^{(e)}_{yx}$, $\gamma^{(e)}_{yz} = -\gamma^{(e)}_{zy}$, but $\gamma^{(e)}_{xz} = \gamma^{(e)}_{zx}$, $\alpha^{(e)}_{xy} = -\beta^{(e)}_{yx}$, $\alpha^{(e)}_{yz} = -\beta^{(e)}_{zy}$, $\alpha^{(e)}_{xz} = \beta^{(e)}_{zx}$. These equalities are in accordance with the generalized Onsager-Casimir reciprocity relations in Eqs. (46)–(48).

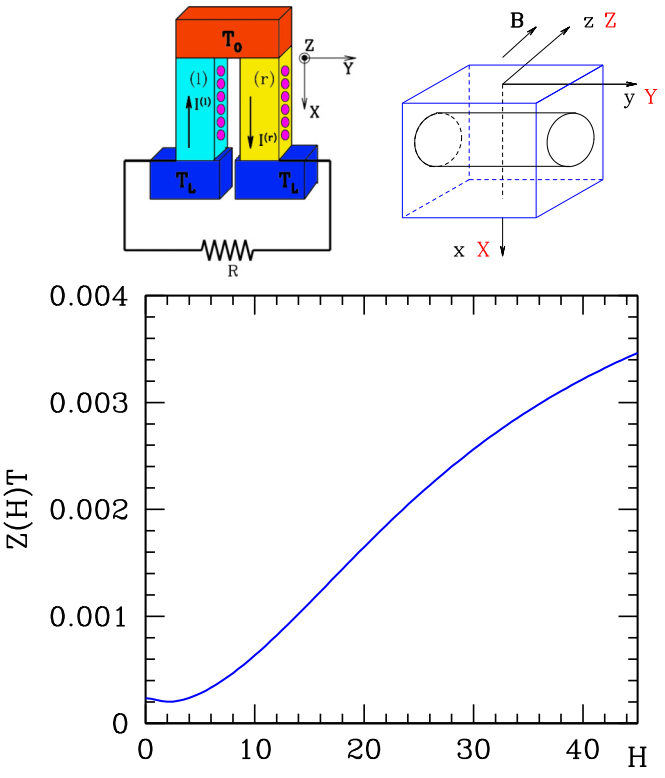

FIG. 11. Longitudinal dimensionless figure of merit $Z(H)T$ [see Eqs. (2)–(49)] of the composite medium with a periodic square array of cylinders (with the y axis perpendicular to the current $\mathbf{I} \parallel X$; see the top of the figure) vs the applied magnetic field H. The effective macroscopic tensor components in Eq. (2) were obtained for the same parameters as in Fig. 5. $T = 300$ K. $\mathbf{H} \parallel z$. In the top left there is a schematic drawing of the thermomagnetic device made from a sample with cylindrical inclusions aligned along y and perpendicular to the current $\mathbf{I}$. In the top right there appears one unit cell of the composite with the orientation of the cylindrical inclusion and direction of the magnetic field $\mathbf{B}$. The coordinate axes X,Y,Z are directed as in Refs. [23,24], while the coordinate axes x,y,z are connected to the composite microstructure (in accordance with Fig. 4).

cases (when the current $\mathbf{I}$ is perpendicular to the axes of the cylindrical inclusions) ZT can increase with H, as shown in Fig. 11.

VII. SUMMARY

The macroscopic response of a two-constituent composite was studied for the case where both constituents have a nonzero Seebeck coefficient and a nonzero Hall resistivity. This was first done for the case of a parallel-slab microstructure where both constituents are isotopic materials and the magnetic field $\mathbf{B}$ is parallel to the slabs. More complicated microstructures were also considered, namely, a simple-cubic periodic array of spherical inclusions and a square array of circular-cylinder inclusions in an otherwise uniform host.

The longitudinal thermoelectric figure of merit ZT (i.e., when the macroscopic electric and thermal currents flow in parallel directions) was calculated for some of these microstructures. In particular, we found that in the special flat-slab case that we considered ZT does not increase with increasing Hall resistivity. By contrast, in the square array of parallel circular cylinders with $\mathbf{B}$ perpendicular to the cylinder axes and the electric and thermal currents perpendicular to both $\mathbf{B}$ and those axes ZT does increase with $\mathbf{B}$.

A general theory was developed and first applied to the flat-slab microstructure and then to two-constituent composites with a spatially periodic microstructure. Detailed numerical computations showed that, like the macroscopic magnetoresistivity tensor computed in earlier studies, the thermoelectric response also becomes strongly dependent on the direction of the magnetic field $\mathbf{B}$ when $|H| > 1$.

Besides obtaining the theoretical results, we have also discussed them for particular choices of the constituents in order to motivate experimental studies of the magnetothermoelectric response of real composites.

All of these studies were carried out for the case where all the microstructural length scales are large enough that the constituents can be fully characterized by the bulk values of their electrical resistivity and thermal resistivity tensors and Seebeck coefficients.

In a future publication we will examine the effect of a strong magnetic field on the properties of a thermoelectric heat pump and thermoelectric heat generator. It will be interesting and useful if it turns out that the figure of merit can be increased above those of the constituents by application of a strong magnetic field to the composite.

Recently, it was shown that one can design metamaterials where the Hall coefficient matrix can be fully controlled [43–45]. This might be another motivation to consider more sophisticated microstructures for a magnetothermoelectric composite.

ACKNOWLEDGMENTS

The research of Y.M.S. was supported, in part, by a grant from the KAMEA program of the Ministry of Absorption of the State of Israel. This work was supported also by the Cy-Tera HPC Project (pro16b108s1), which is cofunded by the European Regional Development Fund and the Republic of Cyprus through the Research Promotion Foundation.

APPENDIX: EXPRESSIONS FOR ZT IN THE CASE OF PARALLEL SLABS

1. Parallel slabs oriented perpendicular to the electric current I

Let the slabs in the system shown in Fig. 2 be oriented perpendicular to the macroscopic electric current $\mathbf{I}$ [see Fig. 1(a)]. Then from Eqs. (18)–(25) it follows that in the device coordinate system $(X,Y,Z) = (z,x,y)$ (note that the x,y,z coordinate axes, in general, do not coincide with the X,Y,Z axes) the macroscopic tensor moduli are

$$\hat{\gamma}_e = \begin{pmatrix} \gamma_{zz}^{(e)} & 0 & 0 \\ 0 & \gamma_{xx}^{(e)} & 0 \\ 0 & 0 & \gamma_{yy}^{(e)} \end{pmatrix}, \quad \hat{\alpha}_e = \begin{pmatrix} \alpha_{zz}^{(e)} & \alpha_{zx}^{(e)} & 0 \\ 0 & \alpha_{xx}^{(e)} & 0 \\ 0 & 0 & \alpha_{yy}^{(e)} \end{pmatrix},$$

$$\hat{\beta}_e = \begin{pmatrix} \beta_{zz}^{(e)} & 0 & 0 \\ \beta_{xz}^{(e)} & \beta_{xx}^{(e)} & 0 \\ 0 & 0 & \beta_{yy}^{(e)} \end{pmatrix}, \quad \hat{\rho}_e = \begin{pmatrix} \rho_{zz}^{(e)} & \rho_{zx}^{(e)} & 0 \\ \rho_{xz}^{(e)} & \rho_{xx}^{(e)} & 0 \\ 0 & 0 & \rho_{yy}^{(e)} \end{pmatrix}.$$

Equation (49) then takes the form

$$ZT = \frac{\alpha_{zz}^{(e)2}}{\gamma_{zz}^{(e)}\left[\rho_{zz}^{(e)} - \left(\frac{\alpha_{zz}^{(e)}\beta_{zz}^{(e)}}{\gamma_{zz}^{(e)}} + \frac{\alpha_{zx}^{(e)}\beta_{xz}^{(e)}}{\gamma_{xx}^{(e)}}\right)\right]}. \tag{A1}$$

Since $\rho_{zz}^{(e)}$ increases drastically with H (positive magnetoresistance; see Fig. 3), the figure of merit ZT decreases with increasing H [see Fig. 3(q)].

2. Parallel slabs oriented parallel to current I ∥ X

Let the slabs in the system shown in Fig. 2 be oriented parallel to the thermoelectric current **I** [see Fig. 1(b)]. Then from Eqs. (18)–(25) it follows that in the device coordinate system $(X,Y,Z) = (x,z,y)$ the macroscopic moduli tensors are

$$\hat{\gamma}_e = \begin{pmatrix} \gamma_{xx}^{(e)} & 0 & 0 \\ 0 & \gamma_{zz}^{(e)} & 0 \\ 0 & 0 & \gamma_{yy}^{(e)} \end{pmatrix}, \quad \hat{\alpha}_e = \begin{pmatrix} \alpha_{xx}^{(e)} & 0 & 0 \\ \alpha_{zx}^{(e)} & \alpha_{zz}^{(e)} & 0 \\ 0 & 0 & \alpha_{yy}^{(e)} \end{pmatrix},$$

$$\hat{\beta}_e = \begin{pmatrix} \beta_{xx}^{(e)} & \beta_{xz}^{(e)} & 0 \\ 0 & \beta_{zz}^{(e)} & 0 \\ 0 & 0 & \beta_{yy}^{(e)} \end{pmatrix}, \quad \hat{\rho}_e = \begin{pmatrix} \rho_{xx}^{(e)} & \rho_{xz}^{(e)} & 0 \\ \rho_{xz}^{(e)} & \rho_{zz}^{(e)} & 0 \\ 0 & 0 & \rho_{yy}^{(e)} \end{pmatrix}.$$

Equation (49) then takes the form

$$ZT = \frac{\alpha_{xx}^{(e)2}}{\gamma_{xx}^{(e)}\left(\rho_{xx}^{(e)} - \frac{\alpha_{xx}^{(e)}\beta_{xx}^{(e)}}{\gamma_{xx}^{(e)}}\right)}. \tag{A2}$$

All the macroscopic moduli that appear in the last equation do not change with H (see Fig. 3); therefore the figure of merit ZT also does not change with H [see Fig. 3(r)].

[1] A. V. Ettingshausen and W. Nernst, Ann. Phys. (Berlin, Ger.) **265**, 343 (1886).
[2] M. C. Steele and J. Babiskin, Phys. Rev. **98**, 359 (1955).
[3] M. C. Steele, Phys. Rev. **107**, 81 (1957).
[4] K. Sugihara, J. Phys. Soc. Jpn. **27**, 356 (1969).
[5] K. Sugihara, J. Phys. Soc. Jpn. **27**, 362 (1969).
[6] K. P. Ghatak and M. Mondal, Phys. Status Solidi B **135**, 819 (1986).
[7] D. V. Gitsu, F. M. Muntyanu, and A. S. Fedorko, Phys. Status Solidi **42**, 173 (1970).
[8] E. Altenkirch, Phys. Z. **10**, 560 (1909).
[9] E. Altenkirch, Phys. Z. **12**, 920 (1911).
[10] A. F. Ioffe, *Semiconductor Thermoelements and Thermoelectric Cooling* (Infosearch, London, 1957).
[11] D. J. Bergman and O. Levy, J. Appl. Phys. **70**, 6821 (1991).
[12] P. J. Lin-Chung and T. L. Reinecke, Phys. Rev. B **51**, 13244 (1995).
[13] D. A. Broido and T. L. Reinecke, Phys. Rev. B **51**, 13797 (1995).
[14] M. Hanabe, S. Yamamoto, S. Yamaguchi, H. Takahashi, H. Okomura, L. Yonenaga, T. Sasaki, and K. Watanabe, Magnetic field effect for Improvement of thermoelectric conversion: A proposal for Nernst-Seebeck element, in *Proceedings of the 22nd International Conference on Thermoelectrics, 2003* (IEEE Press, Piscataway, NJ, 2003), pp. 567–570.
[15] D. M. Rowe, *Thermoelectrics Handbook: Macro to Nano* (CRC Press, Boca Raton, FL, 2005).
[16] T. C. Harman, J. M. Honig, and B. M. Tarmy, Adv. Energy Convers. **5**, 1 (1965).
[17] D. J. Bergman, Thermoelectric tensor and figure of merit for a composite medium: Some exact bounds, in *Proceedings of the 16th International Conference on Thermoelectrics, Dresden, August 26–29, 1997*, edited by A. Heinrich and J. Schumann (IEEE Press, New York, 1997), pp. 401–403.
[18] T. H. H. Vuong, R. J. Nicholas, M. A. Brummell, J. C. Portal, F. Alexandre, J. M. Masson, and T. Kerr, Solid State Commun. **57**, 381 (1986).
[19] J. P. Straley, J. Phys. D **14**, 2101 (1981).
[20] M. Milgrom and S. Shtrikman, Phys. Rev. Lett. **62**, 1979 (1989).
[21] M. Milgrom and S. Shtrikman, Phys. Rev. A **40**, 1568 (1989).
[22] A. Popescu, L. M. Woods, and G. S. Nolas, Phys. Rev. B **85**, 115202 (2012).
[23] T. C. Harman and J. M. Honig, *Thermoelectric and Thermomagnetic Effects and Applications* (McGraw-Hill, New York, 1967).
[24] T. C. Harman, J. M. Honig, and B. M. Tarmy, J. Appl. Phys. **34**, 2215 (1963).
[25] D. J. Bergman and Y. M. Strelniker, Phys. Rev. B **49**, 16256 (1994).
[26] Y. M. Strelniker and D. J. Bergman, Phys. Rev. B **50**, 14001 (1994).
[27] D. J. Bergman and Y. M. Strelniker, Phys. Rev. B **51**, 13845 (1995).
[28] Y. M. Strelniker and D. J. Bergman, Phys. Rev. B **53**, 11051 (1996).
[29] D. J. Bergman and Y. M. Strelniker, Phys. Rev. B **60**, 13016 (1999).
[30] M. Tornow, D. Weiss, K. von Klitzing, K. Eberl, D. J. Bergman, and Y. M. Strelniker, Phys. Rev. Lett. **77**, 147 (1996).
[31] G. J. Strijkers, F. Y. Yang, D. H. Reich, C. L. Chien, P. C. Searson, Y. M. Strelniker, and D. J. Bergman, IEEE Trans. Magn. **37**, 2067 (2001).
[32] D. J. Bergman and L. G. Fel, J. Appl. Phys. **85**, 8205 (1999).
[33] Y. Yang, C. Gao, and J. Li, Acta Mech. **225**, 1211 (2014).
[34] T. C. Harman and J. M. Honig, J. Appl. Phys. **33**, 3188 (1962).
[35] D. J. Bergman and K. J. Dunn, Phys. Rev. B **45**, 13262 (1992).
[36] J. R. Klauder and J. E. Kunzler, in *The Fermi Surface*, edited by W. A. Harrison and M. B. Webb (Wiley, New York, 1960), p. 125.

[37] N. E. Alekseevskii and Yu. P. Gaidukov, Zh. Eksp. Teor. Fiz. **36**, 447 (1959) [Sov. Phys. JETP **9**, 311 (1959)].
[38] M. E. Ertl, D. M. Jacobson, and H. J. Johnson, J. Phys. D **3**, 617 (1970).
[39] L. Onsager, Phys. Rev. **37**, 405 (1931); **38**, 2265 (1931).
[40] H. B. G. Casimir, Rev. Mod. Phys. **17**, 343 (1945).
[41] S. R. de Groot, *Thermodynamics of Irreversible Processes* (North-Holland, Amsterdam, 1951).
[42] Y. M. Strelniker, R. Berkovits, A. Frydman, and S. Havlin, Phys. Rev. E **69**, 065105(R)(2004), and references therein.
[43] C. Kern, V. Schuster, M. Kadic, and M. Wegener, Phys. Rev. Appl. **7**, 044001 (2017).
[44] C. Kern, M. Kadic, and M. Wegener, Phys. Rev. Lett. **118**, 016601 (2017).
[45] M. Kadic, R. Schittny, T. Bückmann, C. Kern, and M. Wegener, Phys. Rev. X **5**, 021030 (2015).